[11] H. S. Sommers, Jr., and E. K. Gatchell, "Demodulation of low-level broad-band optical signals with semiconductors: Part III—Experimental study of the photoconductive detector," *Proc. IEEE*, vol. 54, pp. 1553–1568, Nov. 1966.
[12] E. H. Putley, "Electrical conduction in n-type InSb between 2°K and 300°K," *Proc. Phys. Soc. London*, part 2, vol. 73, pp. 280–290, Feb. 1958.
[13] Y. Yafet, R. W. Keyes, and E. N. Adams, "Hydrogen atom in strong magnetic field," *J. Phys. Chem. Solids*, vol. 1, pp. 137–142, Nov. 1956.
[14] R. J. Sladek, "Magnetically induced banding in n-InSb," *J. Phys. Chem. Solids*, vol. 5, pp. 157–170, May 1958.
[15] I. I. Eldumiati and G. I. Haddad, "Cavity perturbation techniques for measurement of the microwave conductivity and dielectric constant of a bulk semiconductor material," *IEEE Trans. Microwave Theory Tech.*, vol. MTT-20, pp. 126–132, Feb. 1972.
[16] J. J. Whalen and C. R. Westgate, "Temperature dependence of the energy relaxation time in n-InSb," *Appl. Phys. Lett.*, vol. 15, pp. 292–297, Nov. 1969.
[17] C. H. Townes and S. Geschwind, "Limiting sensitivity of a microwave spectrometer," *J. Appl. Phys.* (Corresp.), vol. 19, pp. 795–796, Aug. 1948.
[18] C. F. Krumm, "Millimeter- and submillimeter-wave detection by paramagnetic materials," Electron Phys. Lab., Univ. Mich., Ann Arbor, Tech. Rep. 116, Apr. 1970.
[19] J. G. Ondria, "A microwave system for measurements of AM and FM noise spectra," *IEEE Trans. Microwave Theory Tech.*, vol. MTT-16, pp. 767–781, Sept. 1968.
[20] F. N. H. Robinson, *Noise in Electrical Circuits*. London: Oxford Univ. Press, 1962.
[21] I. I. Eldumiati, "Bulk semiconductor materials for millimeter- and submillimeter-wave detection," Electron Phys. Lab., Univ. Mich., Ann Arbor, Tech. Rep. 118, Dec. 1970.
[22] J. P. McKelvey, *Solid State and Semiconductor Physics*. New York: Harper and Row, 1966.
[23] R. C. Tolman, *The Principles of Statistical Mechanics*. London: Oxford Univ. Press, 1938.
[24] F. J. Low, "Low temperature germanium bolometers," *J. Opt. Soc. Amer.*, vol. 51, pp. 1300–1304, Nov. 1961.
[25] D. H. Martin and D. Bloor, "The application of superconductivity to the detection of radiant energy," *Cryogenics*, vol. 1, pp. 157–165, Mar. 1961.
[26] C. A. Burrus, Jr., "Backward diodes for low-level millimeter-wave detection," *IEEE Trans. Microwave Theory Tech.*, vol. MTT-11, pp. 357–362, Sept. 1963.
[27] Sh. M. Kogan, "A photoconductivity theory based on variations of carrier mobility," *Soviet Phys.—Solid State*, vol. 4, pp. 1386–1389, Jan. 1963.
[28] J. J. Whalen and C. R. Westgate, "Temperature dependence of the conversion loss and response time of InSb mixers," *IEEE Trans. Electron Devices*, vol. ED-17, pp. 310–319, Apr. 1970.

Ion-Implanted Hyperabrupt Junction Voltage Variable Capacitors

R. A. MOLINE, MEMBER, IEEE, AND G. F. FOXHALL, SENIOR MEMBER, IEEE

Abstract—**Voltage variable capacitors have been fabricated using ion implantation and a PtSi Schottky barrier to obtain a high degree of control over the doping in a hyperabrupt diode structure. Three methods for obtaining the desired doping in the hyperabrupt region have been investigated, including diffusion from a low energy predeposition and higher energy implantations with no diffusion.**

The C–V characteristics for two different profiles, made using diffusion to drive in an ion predeposition, agree well with theoretical calculations if a Gaussian diffusion profile peaked at the surface is assumed ($D=2.38\times10^{-13}$ cm²/s for phosphorus at 1100°C in an oxygen ambient). It has been found that the device parameter spread of about 7 percent is dominated by nonuniformities in the donor concentration of the epitaxial layer. Parameter variations due to sources other than the epitaxial layer doping are about 3 percent.

Low-dose channeling implantations have been made to tailor the profile such that the sensitivity $-(dC/C)(V/dV)$ is nearly constant (2.5) over a factor of three change in capacitance.

I. Introduction

HYPERABRUPT junction diodes used as voltage variable capacitors (VVC) are characterized by a rapid decrease in their depletion layer capacitance with increasing reverse bias. Such devices find important application in the design of voltage-controlled resonant circuits that in turn form an integral part of tuners, voltage-to-frequency converters, FM modulators, and other devices [1]. There are numerous other uses for VVC's in nonresonant circuit applications, such as *RC* phase shifters.

One can achieve considerable circuit simplification if predetermined *C-V* characteristics of the VVC can be precisely controlled. This paper describes fabrication techniques using ion implantation [2] that achieve this objective. In addition, the versatility of ion implantation in shaping the device characteristics is demonstrated. First some general features of VVC's are presented. Then theoretical considerations are given for specific parameters. Following this, three different methods of fabrication using ion implantation are given with typical results. Sources of variations in device characteristics are discussed for each of the three methods.

II. Theoretical Considerations

Any reverse-biased junction diode exhibits VVC characteristics. One parameter that is important in characterizing the device is the sensitivity $m(V)$ defined by

$$m = -\frac{dC}{C}\frac{V}{dV} \tag{1}$$

Manuscript received May 26, 1971; revised September 2, 1971.
R. A. Moline is with the Bell Telephone Laboratories, Inc., Murray Hill, N.J. 07974.
G. F. Foxhall is with the Bell Telephone Laboratories, Inc., Reading, Pa. 19604.

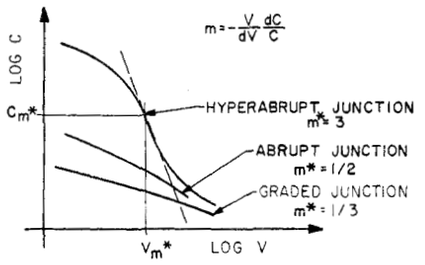

Fig. 1. Capacitance–voltage relationship for linear-graded abrupt and hyperabrupt junction diodes.

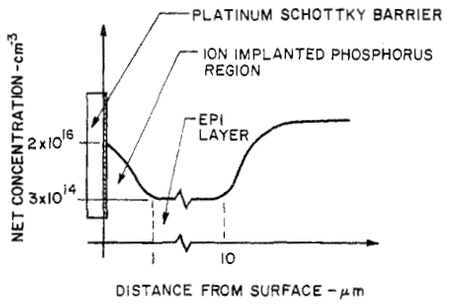

Fig. 2. Schematic representation of the doping profile for a typical hyperabrupt junction diode.

where C is the capacitance of the device and V is the applied reverse bias. This represents the magnitude of the slope of the log C–log V relationship at a given voltage. It is useful to denote the maximum value of m as m^* and the corresponding capacitance and voltage as C_m^* and V_m^*, respectively. This represents the operating point at which m is essentially independent of voltage for small-signal applications.

The C–V relationship of a typical hyperabrupt diode is shown in Fig. 1 and is compared with those for the more familiar linear graded and abrupt junction diodes. For low bias, m is small due to the influence of the self-biasing of the junction. For sensitivities greater than 0.5, one is forced to utilize the hyperabrupt junction structure in which the doping concentration decreases with increasing distance from the junction. To provide this region of decreasing density, a layer of enhanced carrier concentration is introduced near the surface. A typical profile is shown schematically in Fig. 2.

The total amount of charge in this layer is limited by the fact that to deplete 2×10^{12} carriers/cm^2 in silicon, a field of 30 V/μm is needed at the junction. This is near the avalanche field for lightly doped silicon. This complicates the fabrication of the device by conventional techniques since it implies that the sheet resistance of the layer must be greater than $3\times10^3\Omega/\square$ for n-type silicon. The devices reported here have exploited the inherent control using ion implantation to count the number of carriers injected into the region under the junction. To retain this high degree of control for the number of carriers on the finished device, a Schottky-barrier diode was used to form a very shallow junction in lieu of a deeper p-n junction that would compensate some of the implanted charge in a relatively uncontrolled fashion. Considerable insight as to the physical parameters that control the hyperabrupt characteristics of a diode of area A may be gained from the equations

$$m = \frac{-d(\log C)}{d(\log V)} = \frac{-V}{C}\frac{dC}{dV} = \frac{VC^2}{e\kappa\epsilon_0 N(d)A^2} \tag{2}$$

$$V = \frac{e}{\kappa\epsilon_0}\int_0^d\int_{x'}^d N(x)dx\ dx' - V_D \tag{3}$$

$$d = \kappa\epsilon_0 A/C \tag{4}$$

where $x=0$ is the location of the junction, very heavy doping is assumed for $x<0$, the depletion edge is at a depth d, κ is the dielectric constant, e is the magnitude of the electron charge, ϵ_0 is the permittivity of free space, and V_D is the diffusion voltage of the junction. Equations (2) and (3) can be combined to obtain

$$m = \frac{\int_0^d\int_{x'}^d N(x)dx\ dx' - V_D\kappa\epsilon_0/e}{d^2N(d)}. \tag{5}$$

Kennedy *et al.* [3] have shown that N in (2) should really be the equilibrium electron density. In particular, one notes the interdependence of m, C, and V and their critical dependence on the nature of the impurity profile.

A computer program has been written that solves for the majority carrier distribution for an arbitrary impurity profile under a Schottky barrier having a barrier height ϕ. This program is run for zero applied bias on the structure and the C-V characteristics for the hypothetical device are then determined by integrating the majority carrier distribution to obtain the voltage needed to form the depletion edge at various depths d. Comparisons between theory and experiment are shown in Section IV-C.

Quantitative information can be obtained from the above solution but, due to the interdependence of the parameters involved, it is difficult to make broad generalizations as to the behavior of the C-V relationship for arbitrary doping conditions. However, some qualitative generalizations can be made. For example, if all concentration levels are increased by a multiplicative factor F, the value of m^* and C_m^* are unchanged while V_m^* is increased by a factor approaching F for $V_m^* \gg V_D$. For a Gaussian diffusion after a predeposition of charge q, the concentration profile is given by

$$N(x) = \frac{q}{\sqrt{\pi Dt}}\exp\left(-\frac{x^2}{4Dt}\right) + N_B \tag{6}$$

where D is the diffusion constant, t is the diffusion time, and N_B is the background concentration. For $N(0) \gg N_B$, m^* is not a strong function of t while m^* is approximately proportional to q. In general, V_m^* increases with q or t while C_m^* decreases with q or t.

One other parameter of importance for characterization of the device is the quality factor Q. If the shunt resistance of the device is high, then

$$Q = 1/\omega C R_S \tag{7}$$

where R_S is the series resistance of the device and ω is the angular frequency. Equation (7) reduces to

$$Q = d \Big/ \left(\omega \kappa \epsilon_0 \int_d^l \rho \, dx'\right) \tag{8}$$

where l is the thickness of the device and ρ is the resistivity of this layer.

III. Fabrication Techniques

The goal of this program was to study methods for fabricating VVC's with predetermined characteristics. For one particular application, it was required that the following specification be met: 1) $2.5 \leq m^* \leq 4$; 2) $3\ \text{V} \leq Vm^* \leq 5\text{V}$; 3) $7\text{pF} \leq Cm^* \leq 9\ \text{pF}$; and 4) $5 \leq Qm^* \leq 25$ at 100 MHz.

It will be seen that the method described here enables one to fabricate the devices with a narrow spread in parameters within the target region.

From (5) and (6) it is clear that control of the total number of impurities is of first-order importance in the fabrication of the device. Although several techniques have been reported for fabrication VVC's [4]–[7], ion implantation [8] was chosen for this work due to its inherent ability to control the number of atoms in the enhanced region by direct measurement.

For the three fabrication methods described below and in Table I, only the technique of obtaining the final doping profile was altered significantly, with most of the other features remaining identical. The wafers consisted of n-type epitaxial silicon with $N_B = 3 \times 10^{14}\ \text{cm}^{-3}$ and a thickness of 10 μm in the first two methods and bulk material of the same resistivity in the third. After thermal oxidation, boron-doped guard rings 3 μm deep and with 14- or 16-mil nominal diameter were diffused for the first two methods, with a window of corresponding diameter concentric with the guard ring opened subsequently for the implant. The guard ring was not included in the third method. Once the desired enhancement profile was obtained, a PtSi Schottky barrier junction [9] was formed. The PtSi thickness was made less than 250 Å to eliminate variations due to the removal of a fraction of the enhancement layer.

The first method of depositing the enhanced layer involved a hybrid technique in which approximately 1×10^{12} phosphorus ions/cm^2 were deposited at a low energy (50 keV), followed by a diffusion at 1100°C in an O_2 ambient to obtain the desired profile. The second method used a single 300-keV phosphorus implant in a direction off any low index channel to obtain the desired doping profile. The third method was a variation of the second in which the samples were first implanted with 300-keV phosphorus ions in a random direction as above. After the 300-keV implant, 300- and 600-keV ions were injected along the ⟨111⟩ crystal axis to tailor the doping profile, reducing m^* [see (5)]. This method utilized the deeper penetration of ions due to ion channeling [10]. An annual at 700°C for 30 minutes was used for the nondiffused samples to render the donors electrically active [11].

TABLE I
Process Summary for the Three Fabrication Methods

Method	1	2	3
Wafer	Epitaxial	Epitaxial	Bulk
N_B	$3 \times 10^{14}\text{cm}^{-3}$	$3 \times 10^{14}\text{cm}^{-3}$	$3 \times 10^{14}\text{cm}^{-3}$
Guard Ring	Yes	Yes	No
Enhanced Layer	Ion Predeposition	Single Implantation	Multiple Implantations
Diffusion	1100°C, O_2	None	None
Anneal	None	700°C	700°C

IV. Hybrid Results

Although the second and third methods described above give excellent results, the major portion of the effort was directed toward the fabrication of devices by the first method since it requires little control of the implantation parameters other than dose. Two samples 17A and 17B, consisting of adjacent halves of one epitaxial wafer, were processed at separate times through all steps of the fabrication procedure. Each was implanted to a dose of $9.0 \times 10^{11}\ \text{cm}^{-2}$ at 50 keV, with subsequent diffusion for 60 minutes at 1100°C in oxygen prior to application of the PtSi Schottky barrier.

A. Parameter Distributions

Distributions of m^* for 50 devices randomly selected from each sample are shown in Fig. 3. One notes that the means of these distributions differ by about 11 percent and have relatively wide sigmas (Gaussian standard deviation) of 7.0 and 5.8 percent, respectively. While this variation is quite acceptable within the framework of the specification given above, it is illuminating to consider its origins.

The composite distribution of epitaxial layer doping N_B for all 100 devices from the two samples is shown in Fig. 4. One sees that there is not only a wide spread, but, even more striking, there is a clear distinction between the two groups as well. Almost without exception, devices from 17A represent the lower half of the distribution and devices from 17B represent the upper half. The crossover point was found to fall at 3.9×10^{14} cm^{-3}. Evidently the cut made in forming the two halves was essentially perpendicular to a resistivity gradient across the original wafer.

As is implied by (5), the epitaxial layer doping density is a key variable with which m^* varies inversely. One can partially remove this factor by considering devices lying in the restricted background doping range of $3.6 \times 10^{14}\ \text{cm}^{-3}$ to $4.2 \times 10^{14}\ \text{cm}^{-3}$. This allows one to obtain some measure of the consistency of the

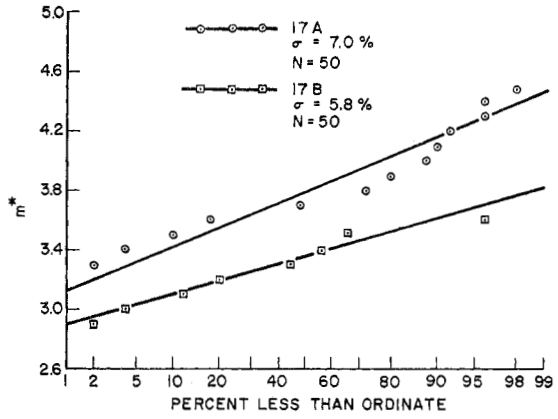

Fig. 3. Distributions of m^* for 17A and 17B using 50 randomly selected devices from each.

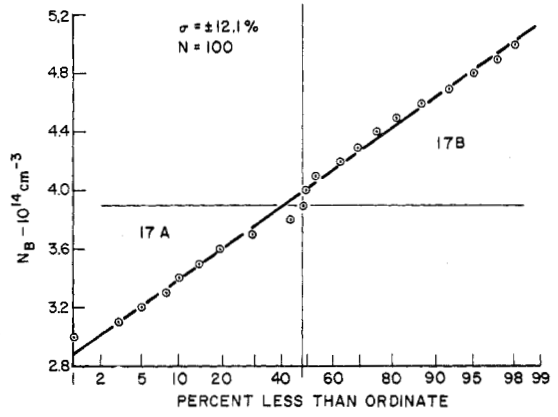

Fig. 4. Distribution of background doping density for samples 17A and 17B collectively using 100 randomly selected devices.

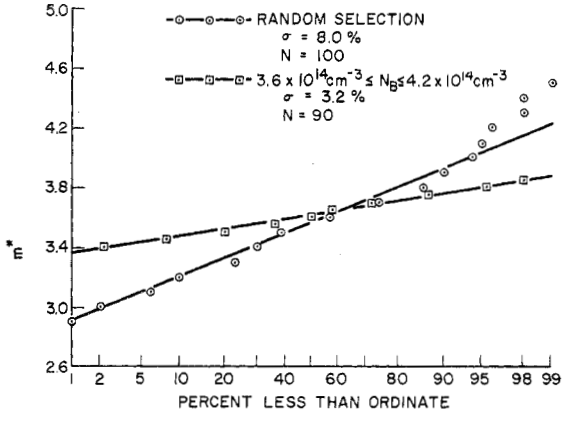

Fig. 5. Comparision of distributions of m^* from 17A and 17B collectively for random selection and restricted selection of background doping.

implantation–diffusion process itself. For example, distributions for m^* for the two groups collectively are shown in Fig. 5 for both random selection and restricted background doping.

It should be noted that both distributions are normal and that the doping restriction drops the sigma from 8.0 to 3.2 percent. This demonstrates that background doping variations play a predominant role in controlling variations in m^* and also that both halves were treated in the same manner throughout the implantation–diffusion process. The latter point is quite important since it shows that radical shifts in parameters due to fluctuations in net charge or PtSi thickness are not to be expected.

TABLE II
METHOD 1—TYPICAL PARAMETER DISTRIBUTIONS

	17A (percent)		17B (percent)		17A, B (percent)	
All Devices	m^*	7.0	m^*	5.8	m^*	8.0
	Vm^*	4.4	Vm^*	3.2	Vm^*	5.2
	Cm^*	4.0	Cm^*	2.9	Cm^*	4.8
	N_B	6.4	N_B	6.4	N_B	12.1
Select N_B	m^*	2.7	m^*	2.3	m^*	3.2
	Vm^*	3.4	Vm^*	3.0	Vm^*	3.4
	Cm^*	3.0	Cm^*	1.5	Cm^*	3.5
	N_B	2.4	N_B	2.4	N_B	6.8

The parameter distributions are summarized in Table II for both random and restricted selection of devices from 17A, 17B, and their composite. This shows that a sigma of typically 3 percent or less may be expected due to variations other than background doping. From (5) and (6), a lower limit on the parameter spread of m^* and Vm^* is given by the sigma of the number of atoms in the predeposited phosphorus layer. Independent experiments utilizing sheet resistance measurements have demonstrated a sigma of only 1 percent for the implanted dose [12]. Of course, other variables such as unintentional contamination of the surface with dopant atoms, variations in the diffusion profile across the wafer, etc., will all tend to increase the parameter spread. Recent experiments have indicated that spurious doping from the back-diffused substrate during the diffusion cycle account for the remaining portion of the variation. Protection of the back surface with oxide (originally removed for contacting during the implant) should eliminate this problem.

B. Aging

Reliability of the ion-implanted, Schottky-barrier structure was determined for conditions of elevated temperatures at a reverse bias of 10 V. By scrupulously controlling the ambient temperature and diode bias during measurement, changes in capacitance of 0.001 pF could be detected, with the devices being held permanently in special fixtures throughout the experiment. It was found that the device capacitance drifted downward with time at a given temperature in a well-behaved, approximately linear fashion. After a change of 0.01 pF out of the nominal capacitance of 2 pF, a device was said to have failed. Life regression curves are shown in Fig. 6. The expected failure rate for use conditions of 50°C and $V_R = Vm^*$ is less than one failure in 10^9 hours of operation.

C. Computer Simulations

The computer program mentioned in Section II was used to calculate C-V characteristics for a structure

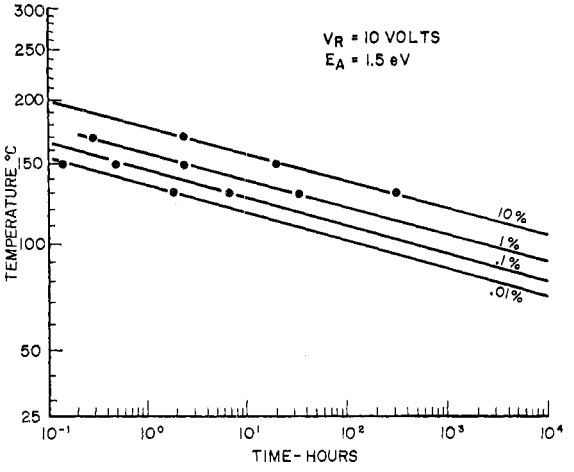

Fig. 6. Biased temperature aging curves, $V_R = 10$ V, endpoint $|\Delta C| = 0.01$ pF, for four different percentage failed.

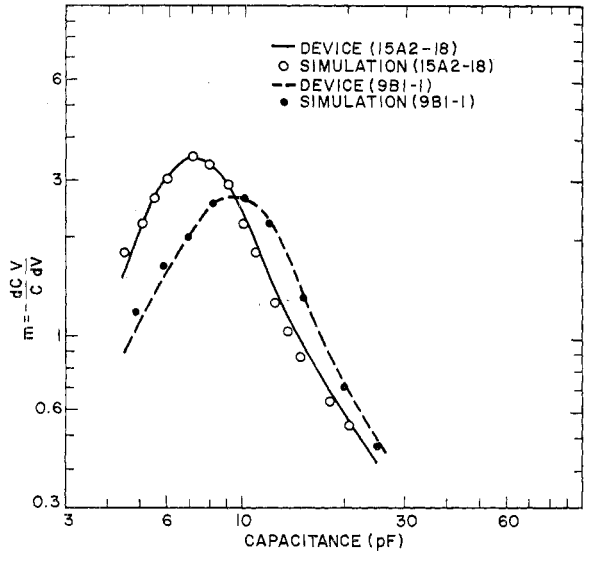

Fig. 7. Comparison of simulated and measured results for two hybrid fabrication conditions.

having the impurity distribution given in (6). The agreement between the calculated and measured sensitivity m as a function of capacitance is shown in Fig. 7 for two different structures. Sample 15A2-18 was predeposited with 9.2×10^{11} ions/cm^2 and diffused for 60 minutes, while sample 9B1-1 was predeposited with 7.5×10^{11} ions/cm^2 and diffused for 34 minutes. The only free parameters in the fit are the diffusion constant D and the background doping N_B. Both calculations required a diffusion constant of 2.38×10^{-13} cm^2/s (for phosphorous diffused at 1100° in an O_2 ambient). N_B for 15A2-18 was 2.6×10^{14} donors/cm^3, while N_B for 9B1-1 was 3.0×10^{14}/cm^3.

V. Ion-Implanted Results

When monoenergetic ions are incident on a noncrystalline sample, they come to rest forming an impurity distributiion that has a peak at a depth R_p, and a characteristic Gaussian shape. The mechanisms and detailed parameters associated with the slowing down

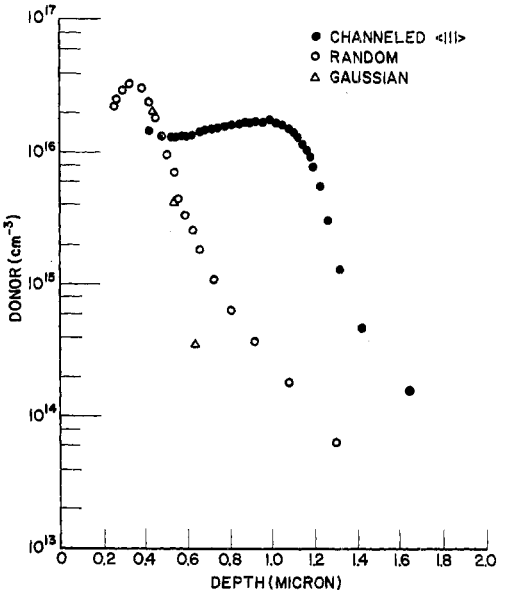

Fig. 8. Donor profile for 300 keV, ^{31}P ions (●) channeled along the ⟨111⟩ direction, (○) implanted in a direction that avoids any major axis or plane ("random direction"), and (△) a Gaussian function that can be compared to the random direction implantation.

of the ions are discussed elsewhere [10]. The impurity profile for $\sim10^{12}$ ^{31}P/cm^2 implanted into a silicon crystal are reported elsewhere [11] and the features that are important here are summarized below.

1) After an anneal at 700°C for 30 minutes, the implanted ions are essentially all electrically active [11].

2) For an implant that is well removed from any low index axis or plane, the concentration profile is nearly Gaussian, with a peak depth equal to 1.1 μm/MeV of beam energy in the energy range of interest here. The profile, as shown in Fig. 8, exhibits a deviation from the Gaussian shape in the form of an exponential decay (tail) at depths beyond the peak and the fraction of implanted charge in this tail appears to be material dependent.

3) For an implant parallel to the ⟨111⟩ axis, the profile is nearly rectangular between 0.3 and 1.2 μm for 300-keV ions and between 0.6 and 1.7 μm for 600-keV ions.

A. Single Implantations

Fig. 9 shows the spread in m^* for a slice in which the enhanced layer was formed by implanting 8×10^{11}, 300 keV ^{31}P/cm^2 into the Si crystal, $\sim7°$ off the ⟨111⟩ axis. The VVC is particularly sensitive to the detailed profile characteristics at a depth where the concentration density has decreased to $\approx1/100$ of the peak density. Since the origin of this tail is not completely understood [11] (although both accidental channeling of beam particles and nonthermal diffusion of the implanted impurities will contribute to it), the narrow spread of m^* shown in Fig. 9 for the restricted background doping results (1.7 percent) is not always observed. It should also be noted that this particular

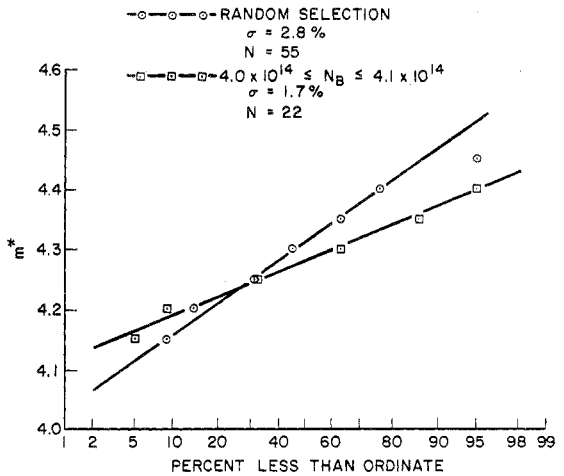

Fig. 9. Comparison of distributions of m^* from a single implant wafer for random selection and restricted selection of background doping.

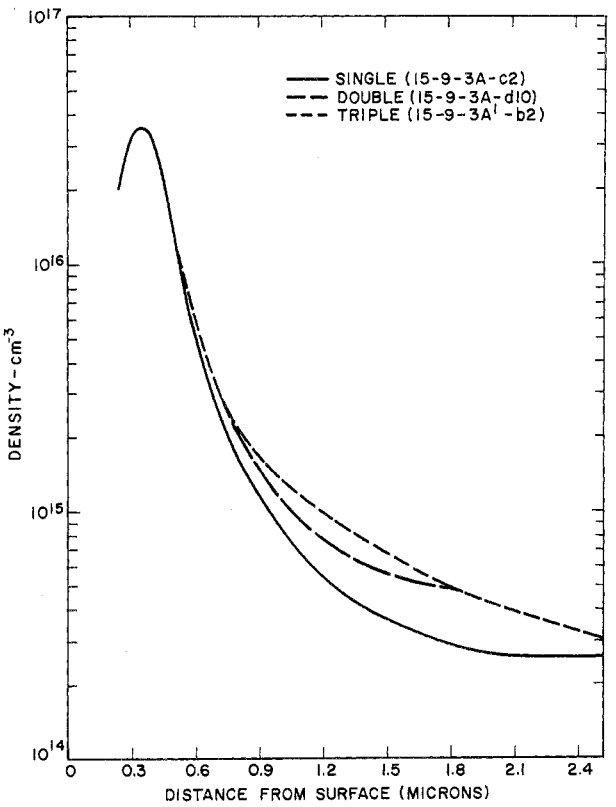

Fig. 10. Doping profiles for single and multiple implant structures.

epitaxial sample had a very narrow spread in its background resistivity.

B. Multiple Implantations

One major advantage of using ion implantation to generate the depth distribution of the enhanced region is that the profile can be tailored using multiple implantations to obtain improved device characteristics. Fig. 10 shows the carrier distributions formed by implanting:

1) $\sim 10^{12}$, 300 keV P/cm², implanted $\sim 7°$ off the ⟨111⟩ axis;

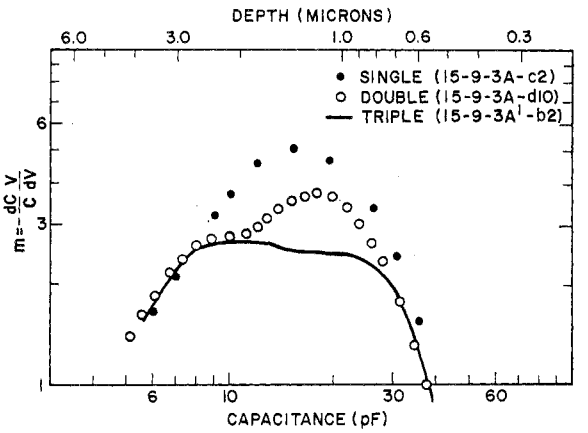

Fig. 11. Sensitivity versus capacitance for single and multiple implant structures.

2) the former 1) plus $\approx 4 \times 10^{10}$, 600 keV P/cm², implanted parallel to the ⟨111⟩ axis; and

3) the former 2) plus $\approx 6 \times 10^{10}$, 300 keV P/cm², implanted parallel to the ⟨111⟩ axis.

Fig. 11 shows the sensitivity m as a function of capacitance for these three profiles. The multiple implants had the predicted effect, lowering m at capacitances that correspond to depths where the doping had a significant influence on the final distribution. This result provides graphic proof of the influence of minor profile changes on the value of m^*, since the two tailoring implants represent a 10 percent perturbation on the integral of the initial implanted charge.

VI. Conclusions

It has been demonstrated that ion implantation, coupled with a drive-in diffusion, offers a technique for fabricating *VVC*'s with predictable and reproducible characteristics. Also, additional flexibility in shaping the *C-V* characteristics can be obtained using multiple implantations.

The requirements placed on the device will dictate which method is employed in its fabrication. If the *C-V* relationship is specified over a limited span of the total potential dynamic range of the device, or if device to device uniformity is the primary goal, then the first method outlined using the implantation as a predeposition is to be preferred since the demands placed on the accelerator are considerably greater for the other fabrication methods. If a preselected constant sensitivity is required over the dynamic range of the device, or more flexibility is required in the *C-V* relationship, then the third method of multiple implantations provides a method for achieving this goal.

References

[1] M. H. Norwood and E. Shatz, "Voltage variable capacitor tuning: A review," *Proc. IEEE*, vol. 56, pp. 788–798, May 1968.
[2] G. F. Foxhall and R. A. Moline, "Advantages of ion-implantation in fabricating hyperabrupt diodes," presented at the IEEE Int. Electron Device Meeting, Washington, D.C., Oct. 1969.
[3] D. P. Kennedy, P. C. Murley, and W. Kleinfelder, "On the measurement of impurity atom distributions in silicon by the differential capacitance technique," *IBM J. Res. Develop.*, pp. 399–409, Sept. 1968.
[4] A. Shimizu and J. Nishizawa, "Alloy-diffused variable capac-

itance diode with large figure-of-merit," *IRE Trans. Electron Devices*, vol. ED-8, pp. 370–377, Sept. 1961.
[5] M. Shinoda, "Capacitance of the hyperabrupt junction fabricated with alloy diffusion technique," *J. Inst. Electron. Commun. Eng., Jap.* (Abstracts), vol. 47, no. 3, pp. 14–15, 1964.
[6] T. Sukegawa, K. Fujikawa, and J. Nishizawa, "Silicon alloy-diffused variable capacitance diode," *Solid-State Electron.*, vol. 6, no. 1, pp. 1–24, 1963.
[7] S. Nakanuma, "Silicon variable capacitance diodes with high voltage sensitivity by low temperature epitaxial growth," *IEEE Trans. Electron Devices*, vol. ED-13, pp. 578–589, July 1966.
[8] P. Brook and C. S. Whitehead, "Hyperabrupt junctions in Au–Si Schottky diodes by ion-implantation," *Electron. Lett.*, vol. 4, no. 16, pp. 335–337, 1968.
[9] M. P. Lepselter and S. M. Sze, "Silicon Schottky barrier diode with near-ideal I-V characteristics," *Bell Syst. Tech. J.*, vol. 47, p. 195, 1968.
[10] J. W. Mayer, L. Eriksson, and J. A. Davies, *Ion-Implantation in Semiconductors*. New York: Academic Press.
[11] R. A. Moline, "Ion-implanted phosphorus in silicon: Profiles using C-V analysis," *J. Appl. Phys.*, Aug. 1971.
[12] R. W. Treible and R. A. Moline, unpublished.

Theory and Experiments on Surface 1/*f* Noise

HORNG-SEN FU, MEMBER, IEEE, AND CHIH-TANG SAH, FELLOW, IEEE

***Abstract*—A theoretical low-frequency noise model for the epitaxial-channel surface field-effect structure is presented where random modulation of the channel conductance arises from fluctuation of charges trapped at the oxide trap states near the Si–SiO_2 interface. In this model, charge fluctuation in the oxide traps arises from carrier tunneling between the fast interface surface states and the oxide trap states. A second fluctuation, at higher frequencies, arises from the random thermal emission and capture of electrons and holes at the fast interface states through the thermal or Shockley–Read–Hall process. Different oxide trap densities were introduced into the interface region of the metal–oxide–silicon field-effect structures using a carefully controlled and reproducible oxygen heat treatment technique. Energy distributions of the oxide trap densities are obtained from capacitance measurements. Humps are observed between the flat band and the onset of strong surface inversion (lower half of the bandgap) in both the noise power and the oxide trap density versus gate voltage (or surface band bending) plots. Theoretical noise power calculations using the experimental oxide trap density profile from the capacitance–voltage data agree very well with the experimental noise humps in both magnitudes and fine structures. It is shown that the frequency spectra of noise depend strongly on the oxide trap density profile in the oxide. It is suggested that the oxide traps are due to the excess oxygen at the SiO_2–Si interface.**

I. Introduction

THE 1/*f* noise has been studied by many investigators. Early studies were primarily on germanium filaments whose surfaces were exposed to different ambients. Many different models have been proposed to explain the noise data [1]–[9]. McWhorter [10] proposed the tunneling model to explain the wide range of frequency spectrum observed in Ge filaments, which has been used by many authors to account for the surface 1/*f* noise in MOS field-effect devices [11]–[18]. In adopting McWhorter's tunneling model, these authors assumed that carriers in conduction or valence bands tunnel directly into the surface states which are located at some energy in the semiconductor bandgap and at some distance away from the interface in the surface oxide. Electron energy of about half of the semiconductor gap (~0.5 eV) must be dissipated. It was shown by Kane [19] that neither the auger-impact mechanism, nor the photon mechanism, nor the multiphoton processes are plausible. Thus, an intermediate state is essential.

In this paper, a new model of carrier tunneling through an intermediate state is proposed that is analogous to the tunneling model used earlier to explain the excess currents observed in gold-doped silicon tunnel diodes [20]. In this model, the carriers in conduction or valence bands communicate with the fast surface states located at the interface through the Shockley–Read–Hall (SRH) process. The carriers then tunnel into or out of the oxide traps located at some distance away from the interface elastically. This model is more plausible than early models since it is well known that the thermal SRH process is very efficient and that continuous (in energy) distribution of fast surface states at the interface is a common characteristic of silicon–silicon-dioxide interface. In this model, a separate time constant for the tunneling process is then obtained, in addition to the Shockley–Read time constant. This is in contrast to the earlier models just referred to where the tunneling process is tacitly absorbed into the Shockley–Read thermal capture rate coefficients.

In getting a correlation between the surface states or oxide traps and the 1/*f* noise, the main difficulty encountered in the previous investigations lies in the lack of detailed data on the spatial and energy distributions of the surface states. A certain type of spatial or energy distribution was generally assumed *a priori* in the earlier work. Recently, Sah and Hielscher [11] have

Manuscript received March 23, 1971; revised September 18, 1971. This work was supported in part by the U. S. Air Force Office of Scientific Research and the Advanced Research Projects Agency. The work is based in part on the doctoral thesis of H. S. Fu submitted to the Graduate College of the University of Illinois, Urbana, Ill.

The authors are with the Department of Electrical Engineering and the Materials Research Laboratory, University of Illinois, Urbana, Ill. 61801.